Combining acoustic black hole and phononic crystal to attenuate structural vibrations

Jean P. C. dos Santos[1], Lucile Naudat[2], José M. C. Dos Santos[1]

[1]*Dept. Computational mechanics,University of Campinas*
Rua Mendeleyev 200, Cidade Universitária Zeferino Vaz, Campinas, SP, Brazil
j265797@dac.unicamp.br, zema@fem.unicamp.br
[2]*ENSIM, University of Maine*
1 Rue Aristote, 72000 Le Mans, France
naudat.lucile.p@gmail.com

Abstract. In the last decades, phononic crystals (PCs) have been investigated extensively and proposed for noise and vibration attenuation, due to the bandgap generated by a destructive wave propagation interference. However, PCs are limited by the characteristic of anisotropy and the periodic cell size that must be of the same order of magnitude as the wavelength in the direction of wave propagation, which are determinants for the band gap width and attenuation. The Acoustic Black Hole (ABH) effect has also been used to attenuate structural vibrations by slowing the waves in a thin-walled structure with a power-law thickness variation. The aim of this paper is to establish reliable numerical approaches for designing and modeling an effective passive structural device combining periodicity and ABH effects to attenuate vibrations efficiently. This structural PC-ABH device is modeled by the Spectral Element (SE) method and verified by the Wave Spectral Element (WSE) method. Simulated examples are performed and the results are compared between the methods and their efficiency to extended band gap widths and to attenuate the structural vibrations are evaluated. .

Keywords: Phononic Crystals, Acoustic Black Hole, Bandgap, Structural vibration.

1 Introduction

Over the last decades, the study of the theory of elastic wave propagation has generated significant interest due to their unique properties and effects and was initiated by Mead [1], that furthermore the Bragg scattering effect was enlightened for revealing the phenomenon of bandgaps, that are Bragg-type forbidden bands in the frequency range allowed for Bragg conditions, and the ability to slow the velocity of sound. In recent decades, phononic crystals (PCs) were conceived with elastic waves propagating in artificially composed periodic structures and received great attention in the mechanical engineering field.

Phononical crystals (PCs) as acoustic or structural metamaterials are artificial periodic composite materials consisting of periodically spaced individuals for creating a unique characteristic of a bandgap that exhibits attenuation in propagation due to the effects of Bragg scattering or local resonance.[2]. The formation of these forbidden bands has been researched in a way to control and manipulate phonons, sound, and other waves, so the ”wave filtering” of the PCs allows different applications in engineering. Furthermore, creating a PC with a full bandgap requires designing different topological structures with different geometric individuals or with different periodic lattices.

Similarly, structures called Acoustic Black Holes are well researched and applied in beams, spirals, tubes and plates for wave attenuation effects in the last four decades. The physical principle first explored by Mironov [3], consists in capturing elastic waves in a geometry with a cross-sectionally varying part whose thickness decreases according to a power-law profile with smoothing criteria of $h(x) = \epsilon x^n$ where n is the power-law ($n \geq 2$), h is the height of the cross-section, ϵ is a constant and x varies from the wedge of the structure. [4]. In recent works, studies have focused on exploring the properties of phononic beams with embedded ABHs for obtaining the bandgaps to improve the effects of wave attenuation. Various notable methods have been proposed to analyze the dynamic

problems with periodic structures, such as the Spectral Element Method and the Wave Spectral Element Method (WSEM).

In this work, an investigation was conducted in a periodic structure with a tapered beam included for wave attenuation, inspired by the ABH effects. The Spectral Element Method (SEM) and the Wave Spectral Element Method (WSEM) were employed for vibration control, bandgap formation, and parametric variation analysis.

2 The Proposed Structure and Methods Applied

This section shows the simplified basic structure evaluated in this work represented in Figure 1 and the formulation utilized for modeling the ABH by the SEM and WSEM methods. The model consists of a structure composite of two ABH elements facing each other and one uniform beam at each end of the structure, containing in total five nodes and 2 degrees-of-freedom (DOFs) per node. The structure can be arranged in the form of a $1 \times n$ matrix, where n represents the periodic expansion of the structure in the x direction. The total length of the cell is defined by equation 1.

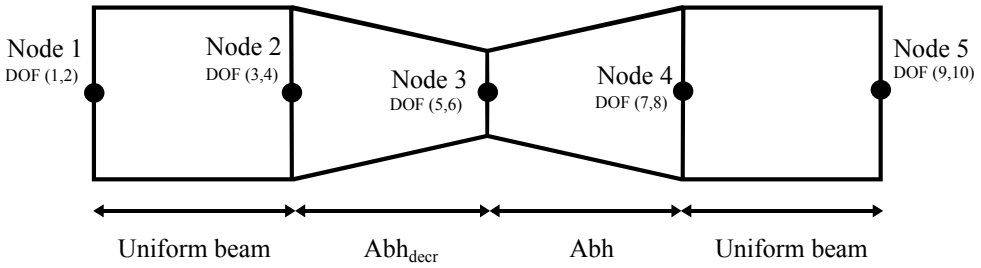

Figure 1. Structural periodic model proposed.

$$L = 2.(L_{abh} + L_{beam}) \tag{1}$$

2.1 Tapered Beam Spectral Model

The ABH model consists of a tapered beam spectral element ([5]) with two nodes with 2 DOFs/node. The Fig. 2 showns the spectral model of the ABH with length L, displacements $\{w_1, \theta_1, w_2, \theta_2\}$ and forces $\{V_1, M_1, V_2, M_2\}$ in node 1 and 2 respectively. The relation within the cross-section areas of the two nodes is given by the amplifying factor $c > -1$ that varies $(1 + c)$ from node 1 to node 2 in the cross-section area $A(x) = A_1(1 + c(x/L))^n$ and in the inertial moment $I(x) = I_1(1 + c(x/L))^{n+2}$, where n is the power-law, that defines the profile of the structure, as shown in Fig. 3a-b

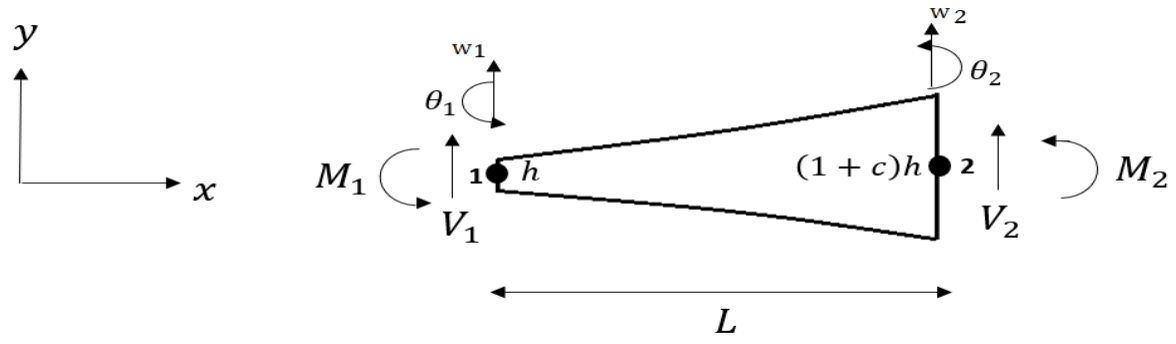

Figure 2. Tapered beam model with two nodes by SEM.

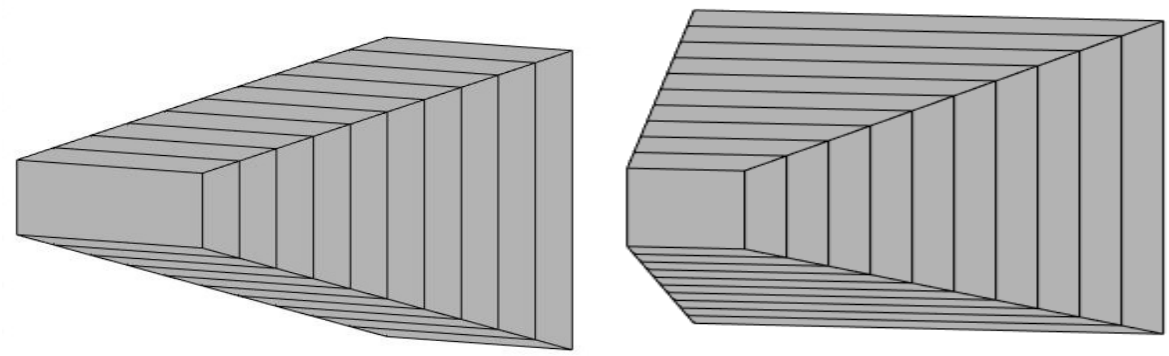

(*a*) (*b*)

Figure 3. Different profiles of the tapered beam model defined by n value for: (a) $n = 1$, (b) $n = 2$.

Taking in consideration the general balance equation of the beam, the solution for a tapered beam case is defined by

$$W(\phi) = \frac{1}{\phi^n}\{C_1 J_n(\phi) + C_2 Y_n(\phi) + C_3 I_n(\phi) + C_4 K_n(\phi)\}, \tag{2}$$

where $\phi = (2\lambda_1/c)\sqrt{\xi}$ with $\lambda_1 = L\sqrt[4]{\rho A_1 \omega^2/EI_1}$, $\xi = 1 + c(x/L)$, $C_i (i = 1, \ldots, 4)$ are constants and J, Y, I, K are Bessel functions of the first, second, first modified and second modified types respectively. Through the derivations of the displacement equations, the angular displacement, bending moment, and shear force are written as:

$$\theta(\xi) = -\frac{\lambda_1}{L\phi^n\sqrt{\xi}}\{C_1 J_{n+1} + C_2 Y_{n+1} - C_3 I_{n+1} + C_4 K_{n+1}\}, \tag{3}$$

$$M(\xi) = -\frac{EI_1\xi^{(n+1/2)}{\lambda_1}^3}{L^3\phi^n}\{C_1 J_{n+1} + C_2 Y_{n+1} + C_3 I_{n+1} + C_4 K_{n+1}\}, \tag{4}$$

$$V(\xi) = -\frac{EI_1\xi^{(n+1)}{\lambda_1}^2}{L^2\phi^n}\{C_1 J_{n+2} + C_2 Y_{n+2} + C_3 I_{n+2} - C_4 K_{n+2}\}. \tag{5}$$

Applying the boundary conditions for displacements in each node and substituting in Eq.2, obtain

$$\underbrace{\begin{Bmatrix} w_1 \\ \theta_1 \\ w_2 \\ \theta_2 \end{Bmatrix}}_{\mathbf{u}} = \underbrace{\begin{bmatrix} \gamma_1 J_n(\alpha) & \gamma_1 Y_n(\alpha) & \gamma_1 I_n(\alpha) & \gamma_1 K_n(\alpha) \\ -\delta_1 J_{n+1}(\alpha) & -\delta_1 Y_{n+1}(\alpha) & \delta_1 I_{n+1}(\alpha) & -\delta_1 K_{n+1}(\alpha) \\ \gamma_2 J_n(\beta) & \gamma_2 Y_n(\beta) & \gamma_2 I_n(\beta) & \gamma_2 K_n(\beta) \\ -\delta_2 J_{n+1}(\beta) & -\delta_2 Y_{n+1}(\beta) & \delta_2 I_{n+1}(\beta) & -\delta_2 K_{n+1}(\beta) \end{bmatrix}}_{\mathbf{A}} \underbrace{\begin{Bmatrix} C_1 \\ C_2 \\ C_3 \\ C_4 \end{Bmatrix}}_{\mathbf{c}}, \tag{6}$$

where $\alpha = 2\lambda_1/c$, $\gamma_1 = 1/\alpha^n$, $\delta_1 = \lambda_1/(L\alpha^n)$ are equations defined for node 1 and $\beta = \alpha\sqrt{(1+c)}$, $\gamma_2 = 1/\beta^n$, $\delta_2 = \lambda_2/(L\beta^n)$, $\lambda_2 = \lambda_1/\sqrt{(1+c)}$ are defined for node 2. Similarly, applying the boundary conditions for the forces in each node and replacing in Eq. 4 and 5, gives

$$\underbrace{\begin{Bmatrix} V_1 \\ M_1 \\ V_2 \\ M_2 \end{Bmatrix}}_{\mathbf{f}} = \underbrace{\begin{bmatrix} \sigma_1 J_{n+1}(\alpha) & \sigma_1 Y_{n+1}(\alpha) & \sigma_1 I_{n+1}(\alpha) & -\sigma_1 K_{n+1}(\alpha) \\ -\tau_1 J_{n+2}(\alpha) & -\tau_1 Y_{n+2}(\alpha) & -\tau_1 I_{n+2}(\alpha) & -\tau_1 K_{n+2}(\alpha) \\ -\sigma_2 J_{n+1}(\beta) & -\sigma_2 Y_{n+1}(\beta) & -\sigma_2 I_{n+1}(\beta) & -\sigma_2 K_{n+1}(\beta) \\ \tau_2 J_{n+2}(\beta) & \tau_2 Y_{n+2}(\beta) & \tau_2 I_{n+2}(\beta) & \tau_2 K_{n+2}(\beta) \end{bmatrix}}_{\mathbf{B}} \underbrace{\begin{Bmatrix} C_1 \\ C_2 \\ C_3 \\ C_4 \end{Bmatrix}}_{\mathbf{c}}, \tag{7}$$

where $\tau_1 = EI_1\lambda_1^2\gamma_1/L^2$, $\sigma_1 = \tau_1\lambda_1/L$, $\tau_2 = EI_2\lambda_2^2\gamma_2/L^2$, $\sigma_2 = \tau_2\lambda_2/L$. Doing $\mathbf{c} = \mathbf{A}^{-1}\mathbf{u}$. and substituting in Eq.(6), is obtained $\mathbf{f} = \mathbf{B}\mathbf{A}^{-1}\mathbf{u}$ that can be rewritten as $\mathbf{D} = \mathbf{B}\mathbf{A}^{-1}$ that represents the spectral dynamic stiffness

of the tapered beam:

$$\mathbf{D} = \begin{bmatrix} d_{11} & d_{12} & d_{13} & d_{14} \\ & d_{22} & d_{23} & d_{24} \\ sym & & d_{33} & d_{34} \\ & & & d_{44} \end{bmatrix}, \tag{8}$$

where the matrix terms can be seen in [5].

For a reverse modelling of the tapered beam, that is, the decreasing pattern that is shown in Fig.2, the positioning of the elements is switched in Eq. (8), that gives the matrix $\mathbf{D_{decr}}$ defined by

$$\mathbf{D_{decr}} = \begin{bmatrix} d_{33} & d_{34} & d_{31} & d_{32} \\ d_{43} & d_{44} & d_{41} & d_{42} \\ d_{13} & d_{14} & d_{11} & d_{12} \\ d_{23} & d_{24} & d_{21} & d_{22} \end{bmatrix}, \tag{9}$$

2.2 Periodic Tapered Beam Model

For solving periodic structure problems, one of the most efficient methods is the application of the Wave Spectral Element Method (WSEM) for finding solutions of the whole structure with low computational cost, where by calculating the dispersion diagram it will be possible to analyze the forbidden gaps (bandgaps), by Floquet-Block periodicity. Considering the Wave Finite Element Method (WFEM) developed by Mencik [6], in the same way the WSEM utilizes a wave propagation approach in a periodic structure. In Eq.(8), the structure is separated into inner degrees of freedom defined by i, the left ones by l and right ones by r.

$$\begin{bmatrix} \mathbf{D_{ii}} & \mathbf{D_{il}} & \mathbf{D_{ir}} \\ \mathbf{D_{li}} & \mathbf{D_{ll}} & \mathbf{D_{lr}} \\ \mathbf{D_{ri}} & \mathbf{D_{rl}} & \mathbf{D_{rr}} \end{bmatrix} \begin{Bmatrix} \mathbf{u_i} \\ \mathbf{u_l} \\ \mathbf{u_r} \end{Bmatrix} = \begin{Bmatrix} \mathbf{0_i} \\ \mathbf{F_l} \\ \mathbf{F_r} \end{Bmatrix} \tag{10}$$

Reducing its order, the condensed stiffness matrix is given by

$$\begin{bmatrix} \mathbf{D_{ll}} & \mathbf{D_{lr}} \\ \mathbf{D_{rl}} & \mathbf{D_{rr}} \end{bmatrix} \begin{Bmatrix} \mathbf{u_l} \\ \mathbf{u_r} \end{Bmatrix} = \begin{Bmatrix} \mathbf{F_l} \\ \mathbf{F_r} \end{Bmatrix} \tag{11}$$

where $\mathbf{D_{ll}} = \mathbf{D_{ll}} - \mathbf{D_{li}}\mathbf{D_{ii}^{-1}}\mathbf{D_{il}}$, $\mathbf{D_{rl}} = \mathbf{D_{rl}} - \mathbf{D_{ri}}\mathbf{D_{ii}^{-1}}\mathbf{D_{il}}$, $\mathbf{D_{lr}} = \mathbf{D_{lr}} - \mathbf{D_{li}}\mathbf{D_{ii}^{-1}}\mathbf{D_{ir}}$ and $\mathbf{D_{rr}} = \mathbf{D_{rr}} - \mathbf{D_{ri}}\mathbf{D_{ii}^{-1}}\mathbf{D_{ir}}$. In a way to avoid ill-conditioning, according to Zhong and Williams [7] the matrix from Eq.(11) is rewritten as

$$\mathbf{q_l} = \underbrace{\begin{bmatrix} \mathbf{I_n} & 0 \\ -\mathbf{D_{ll}} & -\mathbf{D_{lr}} \end{bmatrix}}_{L_i} \underbrace{\begin{Bmatrix} \mathbf{u_l} \\ \mathbf{u_r} \end{Bmatrix}}_{\xi_i} \quad \text{and} \quad \mathbf{q_r} = \underbrace{\begin{bmatrix} 0 & \mathbf{I_n} \\ \mathbf{D_{rl}} & \mathbf{D_{rr}} \end{bmatrix}}_{N_i} \underbrace{\begin{Bmatrix} \mathbf{u_l} \\ \mathbf{u_r} \end{Bmatrix}}_{\xi_i} \tag{12}$$

where $\mathbf{q_l} = \mathbf{u_l} \ \ \mathbf{F_l}^T$ and $\mathbf{q_r} = \mathbf{u_r} \ \ \mathbf{F_r}^T$. $\mathbf{I_n}$ is the identity matrix with the same order as the degrees of freedom on the left or right side. Taking into account the periodicity of the structure, substituting a relation $\mathbf{q_r}^m = \mathbf{q_l^{m+1}}$ in Eq.12 and applying the Floquet-Bloch theorem, gives:

$$e^{\mu}\mathbf{L_i}\xi_\mathbf{i} = \mathbf{N_i}\xi_\mathbf{i} \tag{13}$$

where $\mu = -jkL$ corresponds to the wave propagation constant with j as imaginary number, k is the wave number , L the length of the cell and $\mathbf{L}\xi_\mathbf{i} - \mathbf{N}\xi_\mathbf{i}$ are the eigenvectors.

3 Numeric Results

In this section, we present the results obtained for the cell constructed using the previously described SEM method.

Table 1. Fixed parameters of the cell

Constitutive relation	Nomenclature	Value	Unit
Mass Density	ρ	7850	kg/m^3
Young's Modulus	E_0	210.10^9	Pa
ABH Length	L_{abh}	40.10^{-2}	m
ABH Height	h_{abh}	10.10^{-3}	m
Beam Length	L_{beam}	40.10^{-2}	m
Amplifying Factor	c	3	$\emptyset$

Table 2. Parameter dependent on the value of the power-low n

Power-law	n	[$\emptyset$]	1	2
ABH Depth	b_{abh}	[m]	20.10^{-3}	5.10^{-3}

The fixed key parameters and dimensions of the cell are summarized in Table 1. All other dimensions directly result from these values. However, one dimension of ABH varies based on the power coefficient n, and these values are described in Table 2.

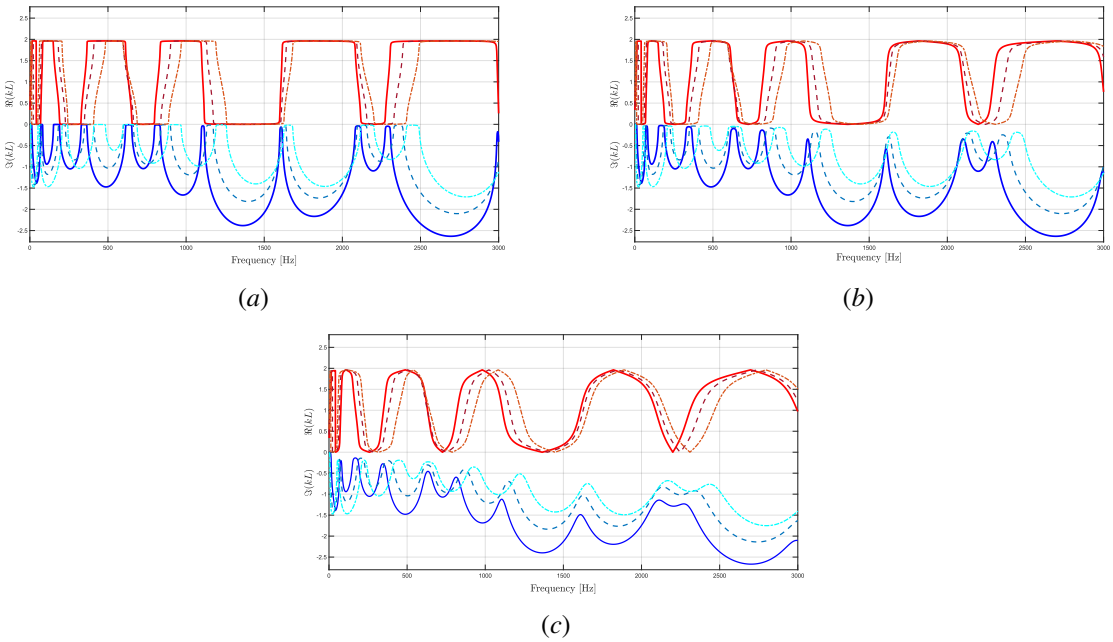

(*a*) (*b*) (*c*)

Figure 4. Dispersion diagram of the cell, with its real part shown in red/orange and its imaginary part in blue, expressed as a function of frequency over a range of 0 to 3000 Hz. Solid lines correspond to dispersion diagrams with $n = 1$, while dashed lines correspond to $n = 2$ and dash-dotted lines to $n = 3$. Additionally, each figure presents the results with a varying loss factor, describing the material of the cell. Figure (a) describes the dispersion diagram with a loss factor of 0.001, figure (b) with 0.01, and figure (c) with 0.05.

On each of these figures, the emergence of band gaps can be observed. These correspond to portions where the real part is nonzero, forming a plateau, while the imaginary part is non-zero and varies according to the frequency. The visibility of the band gaps varies depending on the value of the loss factor. In figure (a), the band gaps are highly pronounced due to a low loss factor (0.001). However, for a loss factor of 0.01, depicted in figure (b), they are much less visible, almost fading away. This is further exemplified in figure (c), illustrating the dispersion diagram with a loss factor of 0.05, where the band gaps are barely noticeable.

Furthermore, we can observe the distinction induced by the power-law factor n. A slight frequency shift between the curves for can be noticed, regardless of the loss factor. For $n = 2$ and $n = 3$, the peaks are shifted towards higher frequencies compared to those for $n = 1$. Additionally, the value of n does not impact the amplitude of the real part, unlike the imaginary part. In the case of $n = 2$ and $n = 3$, the absolute value of the imaginary part

of the dispersion coefficient is higher.

4 Conclusions

An tapered beam proposed as an ABH was modelled with Spectral Element Method, embedded in a periodic structure and was investigated using the Wave Spectral Element Method. The analysis of the dispersion diagram was conducted for the periodic cell with different loss factors and n values, revealing that at higher values of loss factors, the bandgaps are barely noticiable and the results for $n = 2$ and $n = 3$, the peaks shifted to higher frequencies, giving a better result in wave attenuation.

Acknowledgements. The authors are grateful to the Brazilian research funding, FAPESP (Grant No. 15894-0/2018) and CNPq (Grant No. 317436/2021-0).

Authorship statement. The authors hereby confirm that they are the sole liable persons responsible for the authorship of this work, and that all material that has been herein included as part of the present paper is either the property (and authorship) of the authors, or has the permission of the owners to be included here.

References

[1] D. Mead. Free wave propagation in periodically supported, infinite beams. *Journal of Sound and Vibration*, vol. 11, n. 2, pp. 181–197, 1970.
[2] M. I. Hussein, M. J. Leamy, and M. Ruzzene. Dynamics of phononic materials and structures: Historical origins, recent progress, and future outlook. *Applied Mechanics Reviews*, vol. 66, n. 4, 2014.
[3] M. Mironov. Propagation of a flexural wave in a plate whose thickness decreases smoothly to zero in finite interval. *Soviet Physics Acoustics*, vol. 34, pp. 318–319, 1988.
[4] V. Krylov and F. Tilman. Acoustic 'black holes' for flexural waves as effective vibration dampers. *Journal of Sound and Vibration*, vol. 274, pp. 605–619, 2003.
[5] J. R. Banerjee and F. W. Williams. Exact bernoulli-euler dynamic stiffness matrix for a range of tapered beams. *International Journal for Numerical Methods in Engineering*, vol. 21, pp. 2289–2302, 1985.
[6] J.-M. Mencik. *Approche numèrique pour la propagation multi-modale guidèe*. PhD thesis, 2008.
[7] W. Zhong and F. Williams. On the direct solution of wave propagation for repetitive structures. *Journal of Sound and Vibration*, vol. 181, n. 3, pp. 485–501, 1995.